New Perspectives on the Northern Hemisphere Winter Storm Tracks

BRIAN J. HOSKINS

Department of Meteorology, The University of Reading, Reading, United Kingdom

KEVIN I. HODGES

Environmental Systems Science Centre, The University of Reading, Reading, United Kingdom

(Manuscript received 29 January 2001, in final form 14 June 2001)

ABSTRACT

The aim of this paper is to explore the use of both an Eulerian and system-centered method of storm track diagnosis applied to a wide range of meteorological fields at multiple levels to provide a range of perspectives on the Northern Hemisphere winter transient motions and to give new insight into the storm track organization and behavior. The data used are primarily from the European Centre for Medium-Range Weather Forecasts reanalyses project extended with operational analyses to the period 1979–2000. This is supplemented by data from the National Centers for Environmental Prediction and Goddard Earth Observing System 1 reanalyses. The range of fields explored include the usual mean sea level pressure and the lower- and upper-tropospheric height, meridional wind, vorticity, and temperature, as well as the potential vorticity (PV) on a 330-K isentropic surface (PV_{330}) and potential temperature on a PV = 2 PVU surface (θ_{PV2}). As well as reporting the primary analysis based on feature tracking, the standard Eulerian 2–6-day bandpass filtered variance analysis is also reported and contrasted with the tracking diagnostics. To enable the feature points to be identified as extrema for all the chosen fields, a planetary wave background structure is removed at each data time. The bandpass filtered variance derived from the different fields yield a rich picture of the nature and comparative magnitudes of the North Pacific and Atlantic storm tracks, and of the Siberian and Mediterranean candidates for storm tracks. The feature tracking allows the cyclonic and anticyclonic activities to be considered seperately. The analysis indicates that anticyclonic features are generally much weaker with less coherence than the cyclonic systems. Cyclones and features associated with them are shown to have much greater coherence and give tracking diagnostics that create a vivid storm track picture that includes the aspects highlighted by the variances as well as highlighting aspects that are not readily available from Eulerian studies. In particular, the upper-tropospheric features as shown by negative θ_{PV2}, for example, occur in a band spiraling around the hemisphere from the subtropical North Atlantic eastward to the high latitudes of the same ocean basin. Lower-troposphere storm tracks occupy more limited longitudinal sectors, with many of the individual storms possibly triggered from the upper-tropospheric disturbances in the spiral band of activity.

1. Introduction

There have been two basic approaches to diagnosing storm tracks. The first approach identifies the weather systems, tracks their positions with time and produces statistics for their distributions (e.g., Klein 1957), while the second approach is based on determining simple statistics at a set of grid points such as the variance in a frequency band associated with what are considered to be synoptic timescales (e.g., Blackmon 1976; Blackmon et al. 1977). In this paper, in order to illuminate the nature of the Northern Hemisphere winter storm tracks, both techniques are employed on a much wider range of fields than has been considered previously.

Corresponding author address: Dr. Kevin I. Hodges, ESSC, The University of Reading, Harry Pitt Bldg., 3 Earley Gate, Whiteknights, P.O. Box 238, Reading RG6 6AL, United Kingdom.
E-mail: kih@mail.nerc-essc.ac.uk

The feature tracking approach dominated the analysis of the storm tracks from the end of the nineteenth century up until the advent of computers. These early studies were based on a manual analysis using daily synoptic charts. With the introduction of numerical weather prediction gridded analyses covering hemispheric or global regions and for a large number of years, it became more convenient to compute Eulerian statistics to describe the storm tracks such as the variance description already mentioned. The Eulerian approach has dominated until recently due to its ease of application and its provision of a general storm track activity measure. However, Eulerian methods do not tell us everything we might want to know about the types of systems that constitute the storm track activity and most storm attributes can only be speculated at from such statistics. In the last few years, there has been a move back to using feature tracking analysis based on objective, automated methods (e.g., Murray and Simmonds 1991a,b; Lefevre and Niel-

sen-Gammon 1995; Sinclair 1994; Blender et al. 1997; Serreze et al. 1997; Hodges 1994, 1995, 1996) that can provide us with complementary information based on the synoptic systems themselves and allows us to explore the storm track activity according to system type, for example, cyclonic and anticyclonic systems. These methods range from fairly simple nearest-neighbor tracking methods with simple grid box statistics to more sophisticated approaches of tracking and statistical estimation.

In this paper data from the European Centre for Medium-Range Weather Forecasts (ECMWF) have been used for the Northern Hemisphere (NH) winter (December to February). Results will be shown from the application of the filtered variance and tracking techniques to a wide variety of meteorological fields that have important variability in terms of middle-latitude weather systems. Apart from the mean sea level pressure (MSLP) the fields include a number in the lower and upper troposphere and also potential vorticity and potential temperature variables.

The first aim of the paper is to give a broad perspective on the Northern Hemisphere wintertime storm tracks, focusing particularly on a range of feature-tracking diagnostics. The second aim is to use these perspectives to give new insights into possible storm track mechanisms. Although in this paper we concentrate on the NH wintertime storm tracks, in fact all the seasons have been studied, as well as the associated teleconnection activity: these results will be reported in future publications.

In section 2 the data and methodology used will be discussed. In particular, the feature tracking techniques of Hodges (1994, 1995, 1999) will be described as well as the means of determining the statistical diagnostics. The necessity for removing a background flow and the choice made in this work will also be discussed. In section 3 the Eulerian perspective of the NH storm tracks will be presented in terms of the filtered variances while in section 4 the tracking perspective is presented. Finally the results are discussed in section 5 together with some conclusions.

2. Data and techniques

In this section the data used in this study are described as well as the various analysis techniques and the necessity of removing a background field.

a. The data

The primary data used for this study are 6-hourly data for the 22-yr period 1979–2000 and encompass the 15-yr ECMWF Reanalysis (ERA-15; Gibson et al. 1997) supplemented by operational analyses for the later years. Whereas ERA-15 employed an optimal interpolation (OI) data assimilation scheme, the more sophisticated 3D and 4D variational (3D Var and 4D Var) schemes where used for the later operational analyses. One might ask if there are any consequences in using data produced by different data assimilation systems as in the data used here. This does not appear to be a major problem at least at the lower-tropospheric levels with reasonably consistent results obtained from the ECMWF, National Centers for Environmental Prediction (NCEP; Kalnay et al. 1996), and Goddard Earth Observing System 1 (GEOS-1; Schubert et al. 1995) reanalyses, which all used differing flavors of data assimilation. This provides us with some confidence in the reproducibility of these results. However, there is more sensitivity at the upper-tropospheric levels as will be shown later.

The fields that have been examined in this study are much wider ranging than those usually considered using filtered variances or feature tracking methods. For feature tracking, fields have usually been restricted to MSLP, geopotential at 500 hPa (Bell and Bosart 1989) and more recently the lower-tropospheric vorticity ($\boldsymbol{\xi}$), [geostrophic vorticity using MSLP (Sinclair 1994); relative vorticity (Hodges 1996; Ayrault and Joly 2000)]. There are various drawbacks in using these fields. For example, the MSLP is strongly influenced by large spatial scales, such as the Icelandic low, and strong background flows, such as can occur during an enhancement of the subtropical jets, when weak, fast moving synoptic scales can be masked by the background flow until significant development has occurred. Thus the identification of features in unfiltered MSLP tends to be dominated by large-scale features and biased toward the slower moving systems. Additionally the MSLP is an extrapolated field and may be sensitive to how the extrapolation is performed and the representation of the orography in the model. For the 500-hPa geopotential (Z) similar problems can occur as it also is dominated by large spatial scales. Vorticity (ξ) has been found to be a better field for identifying synoptic systems as it is less influenced by the background flow since it focuses on smaller spatial scales and allows systems to be identified much earlier in their life cycle. However, in high-resolution data this field can be very noisy and such structures as frontal systems can begin to be resolved so that for feature tracking some smoothing or reduction in resolution is often required. Additionally if use is made of the geostrophic vorticity computed from the MSLP (Sinclair 1994) this is still dependent on an extrapolated field.

The range of fields explored are listed in Fig. 1, together with the level on which the data were produced and the designation that will be used. This set of fields emphasizes a range of synoptic feature scales, from large (e.g., MSLP and Z) to small [e.g., $\boldsymbol{\xi}$ and potential vorticity (PV)]. At the level of the geostrophic approximation, the focus on smaller spatial-scale features as we move from left to right in Fig. 1 is a consequence of the relevant fields becoming more dependent on higher-order derivatives, which results in smaller spatial scales being enhanced. Some of this range of fields have

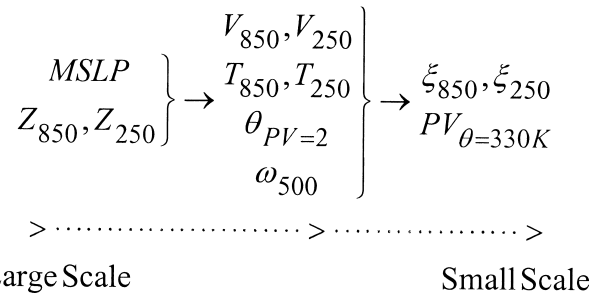

FIG. 1. Fields, level types, level values and designation used for this study: MSLP (MSLP), Z (geopotential), V (meridional wind), T (temperature), θ (potential temperature), ω (vertical velocity), ξ (vorticity), PV (potential vorticity). The suffixes 250, 500, and 850 refer to the pressure levels in hPa. Subsequently the suffixes PV = 2 and θ = 330 K will be reduced to PV2 and 330.

been discussed frequently in Eulerian studies such as that of Hoskins et al. (1989). Other fields such as θ_{PV2}, which is the potential temperature on the PV = 2 PVU surface (PVU = 10^{-6} km^2 kg^2 s^{-1}), are new in this context. It should be noted that away from the deep Tropics the PV = 2 surface can be considered to be a dynamical tropopause (Hoskins and Berrisford 1988; Hoskins 1997). The θ field starts to increase rapidly on this surface as the Tropics are approached and so its value is capped at 380 K.

b. Data preprocessing

The usual approach for identifying midlatitude synoptic features in a gridded data field that are to be tracked is to seek extrema in the field. For some fields such as MSLP and vorticity, extrema can be identified directly. For other fields, such as temperature, the synoptic systems are likely to have an associated extremum only if some background distribution is first removed. In fact even for surface pressure it is debatable whether the movement of low pressure centers into, for example, the Icelandic low is really an artifact of the ambient low pressure there. The range of views are that the Icelandic low is part of a background planetary wave structure associated with the large-scale forcing, or that the Icelandic low is the ensemble of the synoptic lows moving into the region. The most tenable view is probably somewhere in between. As discussed in Anderson et al. (2001a, manuscript submitted to *Mon. Wea. Rev.*, hereafter AHHa) the background distribution can be obtained using either a spatial or temporal filter. Here we take, perhaps, the minimalist approach of removing the planetary scales with total wavenumber (n) less than or equal to 5 from every field at each analysis time, as has been suggested by H. Wernli (1999, personal communication). Many other fields could have more removed without dramatically affecting the structure associated with synoptic weather systems, for example the vorticity, where removing wavenumbers up to 10 does not significantly affect the systems (AHHa). Other fields are more sensitive to the details of the filtering performed, particularly the fields with large to intermediate-scale features. It is shown in AHHa that the more structure that is removed from these fields, the more similar the behavior of positive and negative features becomes. The waveguide behavior found by Wallace et al. (1988) with the 2–6.5-day temporal filter is an example of this. The filtering procedure used here and the sensitivity of the results to the choice made in terms of the wavenumber cutoff are discussed in more detail in AHHa. There it is shown that the simple choice made here of removing wavenumbers less than or equal to 5 is a reasonable, if quite conservative, compromise for all the fields explored.

The data are also truncated at total wavenumber 42 (referred to herein as T42), which is sufficient for identifying synoptic-scale features, and a spectral tapering is performed in order to suppress Gibbs phenomena for all the fields explored. The combination of truncation and spectral tapering makes identifying and tracking the synoptic systems in the noisier, smaller-scale fields easier and more reliable. The form of the taper is that given in Hoskins and Sardeshmukh (1984), acting like a ∇^4 smoother and having a value of 0.1 on the smallest retained scale.

The effect of the preprocessing on a large-scale field is shown in Figs. 2c,d, which show the average of the background and retained components of the MSLP averaged over all the winters. Of course these pictures are equivalent to the $0 \leq n \leq 5$ and $5 < n \leq 42$ parts of the winter mean field. From the above discussion it is perhaps not clear what one would hope to see in the two fields. However, the fact that the high pressure region in the Arctic has a low pressure ''background'' removed means that the retained field tends to have even higher pressure there than in the raw field. This will influence the mean intensities of highs found there but is not serious since few mobile highs are identified in this region. The preprocessing described in this section will in general also be used for the variance analysis as well as the feature tracking. We will show that this has no detrimental effect on the variance perspective.

c. Analysis techniques

The Eulerian diagnostic chosen for this study is the traditional bandpass filtered variance statistic, which will be shown as a standard deviation. For some of the fields such as meridional wind, bandpass filtering is not necessary to obtain all the features relevant to the storm tracks, at least for the Southern Hemisphere (Berbery and Vera 1996). However, for consistency the same procedure is used for each field. The technique used to compute the filtered variance is the periodogram method (Kay 1988), which applies a fast Fourier transform (FFT) to the time series data. The periodogram method is a frequency domain filter as opposed to the often used time domain filtering based on weighted moving av-

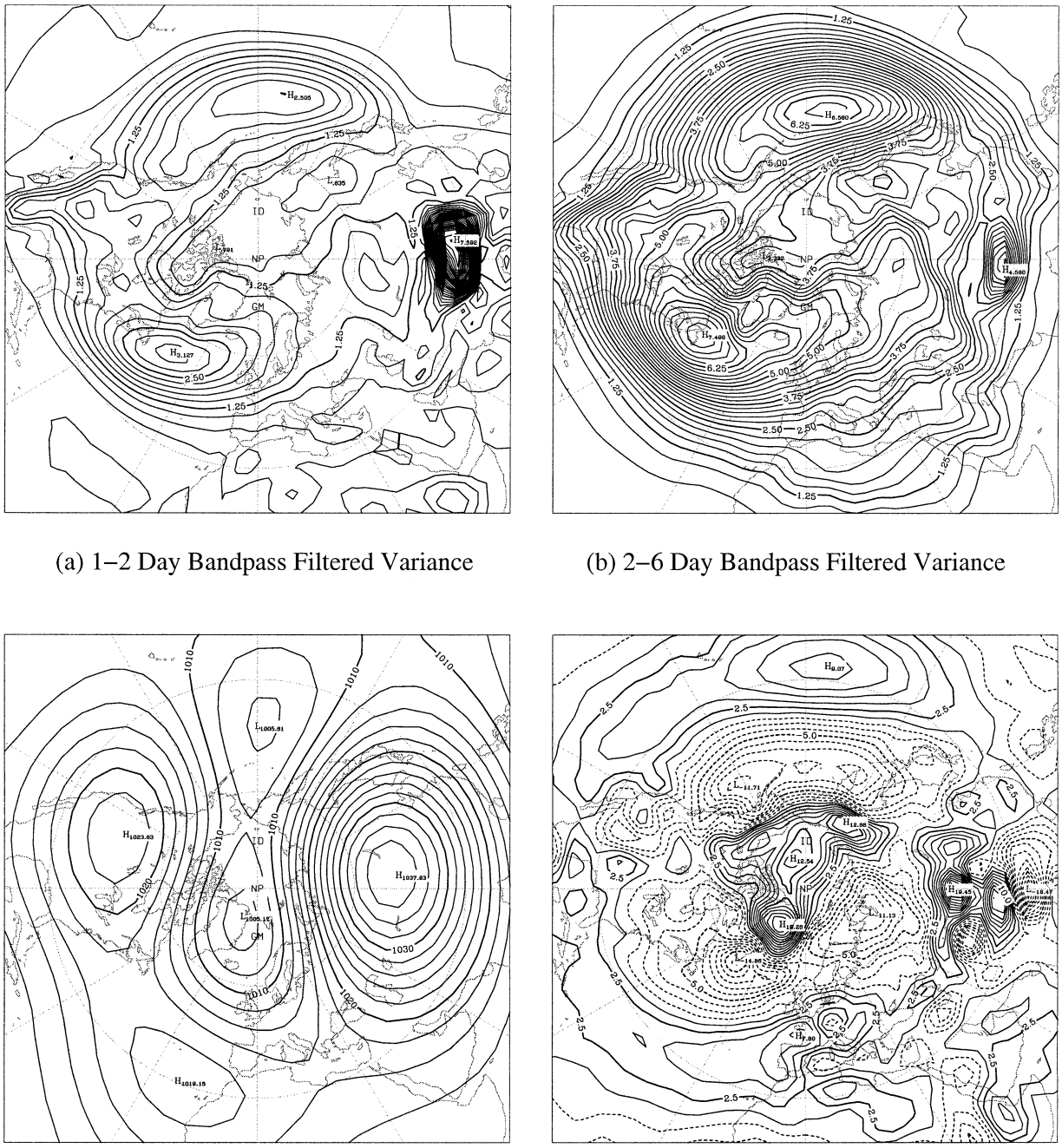

FIG. 2. The MSLP filtered variance converted to std dev in (a) the 1–2-day band and (b) the 2–6-day band, (the contour interval is 0.25 hPa in both), and the winter mean MSLP field split into (c) planetary scale, $0 \leq n \leq 5$ and (d) subplanetary scales, $5 < n \leq 42$, (the contour interval is 5 hPa in both).

erages (Blackmon 1976; Wallace et al. 1988). An example of applying this technique to the MSLP field is shown in Fig. 2b. Investigations were also made as to whether the inclusion of shorter timescales might change the picture presented by the 2–6-day filter and whether 1–6-day filter would be a better choice. This was tested on the MSLP and ξ_{850}. As an example, Fig. 2a shows the 1–2-day standard deviation of MSLP. The general result from both the MSLP and ξ_{850} is that the amplitude and structure in the 1–2-day band are not such as to change the general picture, and so the 2–6-day filter was retained.

As a further check that the removal of the planetary-scale background was not interfering significantly with synoptic timescale variability, the MSLP time-filtered variance was determined without the removal of the planetary-scale background. The result was negligibly different, in accordance with the planetary scales being predominately associated with low-frequency variability (Blackmon 1976).

For the feature tracking approach, having identified maxima or minima in a time series of a field, they must be linked together in time order to form system trajectories. There have been several systems developed to do this, from simple nearest-neighbor searches (Blender et al. 1997; Serreze et al. 1997) to more sophisticated matching techniques (Murray and Simmonds 1991a; Hodges 1994, 1995; Simmonds and Keay 2000). To perform such an analysis for this paper the technique of Hodges (1995) is used. The tracking is performed by minimizing a cost function for the ensemble track smoothness to obtain the minimal set of smoothest tracks. The technique has been generalized to the spherical domain, which obviates the need to use projections, which may introduce systematic bias, and allows the analysis of global data or large spherical regions to be performed. This approach is general and can be applied to a large range of meteorological data.

All tracking techniques impose constraints in one form or another, usually some upper bound on the displacement distance to exclude unlikely matches. The tracking technique used for this work imposes constraints on the track smoothness and on the maximum displacement distance. These are varied adaptively to take account of slow moving and fast moving systems (Hodges 1999). The parameters that are required for the tracking are the intensity threshold (in the filtered field) above which a feature is identified to exist, the maximum displacement distance, and the smoothness demanded of the track. The track ensembles are computed for each winter and then filtered based on the choice of the minimum time of existence (2 days, 8 time steps) and distance moved (10° geodesic, ~1000 km). Finally the filtered track ensembles for each winter are combined to form the 22-yr track ensemble that is used in the statistical estimation of the climatological attributes.

Just as with the tracking, there are a variety of ways of computing the statistics from the feature track ensemble, from the simple grid box counting and averaging methods, which are relatively crude and subject to bias (Taylor 1986; Hayden 1981), to more sophisticated weighting methods based on analytic functions (Murray and Simmonds 1991b). Most previous studies have been performed on projections, which can result in systematic bias even if corrections are made for changes in the sampling regions (area normalization). In this study the approach described by Hodges (1996) is used where the statistics are computed directly on the sphere using spherical kernel estimators with local kernel functions. The use of local kernel functions (as opposed to global exponential functions) makes the estimation much more tractable for large datasets. This approach obviates the need to use projections (apart from display) and negates the need to perform corrections or normalizations. In addition the amount of smoothing of each statistic can be varied adaptively with the local data density, and the global kernel smoothing parameter chosen objectively using cross validation.

A wide range of statistics are computed, including feature, track, genesis, and lysis densities. Except for the track density, the densities are computed as a probability density function (PDF); that is, they integrate to unity on the estimation domain, in this case the NH. The feature density is computed using all points along a track so that for slow moving systems this means a large contribution to the density in a small region due the higher density of points. The track density is computed by using a single point from each track that is closest to the estimation point, the result of this is that the track density is not a PDF but can be normalized to be one. The genesis density, the density of where systems originate, is computed from the starting points of the tracks excluding any tracks that start at the first time step. The lysis density, the density of where systems disappear, is computed from all the end points of the tracks excluding any tracks that end at the last time step. The raw density statistics are subsequently scaled to number densities per month with a unit area equivalent to a 5° spherical cap ($\sim 10^6$ km^2) for analysis and display. Thus all densities will be in units of 10^6 km^2 per month. For the track density two possibilities are available when scaling to number density: either it can first be normalized to a PDF before scaling to a number density, so that the distribution will integrate to the total number of systems (taking account of the area and temporal scaling); or left as the raw statistic and then scaled to number density, which would then integrate to a number greater that the total number of systems, due to the multiple counting. The latter of these is closer to the traditional track density definition of the number of systems passing through a grid box per unit area. In a sense the former is a more global measure of activity while the latter is a more local measure. In this study the latter definition is used. The mean attributes that are computed are for intensity, speed/velocity, growth/decay rates, and lifetime. The mean attributes will not be shown where the feature/track density is low as they will be determined from a small data sample and hence be less reliable. The suppression threshold used for each mean attribute statistic is noted in the figure captions and is chosen subjectively. Note that a feature density suppression threshold applies to the intensity, speed/velocity and growth rates while a track density suppression threshold applies to the lifetimes. Confidence maps could provide a more objective means of delineating the reliability of mean values, and this will be considered for the future but this has not been done here.

3. The Eulerian, filtered variance perspective

The filtered variances considered here are truncated at total wavenumber 21 (T21) and are displayed as standard deviations (std dev) for lower- and upper-tropospheric fields in Figs. 3 and 4, respectively. The T21 truncation is applied to the std dev fields purely for cosmetic purposes to bring out the salient features of the filtered field. Comparison of the MSLP field in Fig. 3a with the T42 version in Fig. 2b shows that there is smoothing without real loss of structure.

The overall impression from Figs. 3 and 4 is one of similarity between the different variables, justifying the notion of storm tracks and of these variables all being good indicators of synoptic activity. However, there are significant and interesting differences in detail.

The Atlantic and Pacific storm track maxima are present for all the variables (for PV_{330} the Pacific maximum is present only without the T21 filter). However, the relative magnitudes of the two maxima depend on the field under consideration. As discussed by Nakamura (1992) the Atlantic is stronger for the standard fields MSLP and Z_{250}. This is also the case for T_{850}, V_{250}, ξ_{250}, and PV_{330}. Indeed the latter two fields give the impression of the central and eastern Pacific being the upstream part of the Atlantic maximum. However, there is approximate equality between the oceanic maxima for Z, V, and ξ at 850 hPa. The vertical velocity at 500 hPa (ω_{500}) shows a slightly stronger Pacific maximum, and θ_{PV2} gives a Pacific maximum more than 20% larger than in the Atlantic. The latter could be explained by the larger meridional gradient of this variable at lower latitudes, this acts to emphasise the Pacific variability, which occurs at a lower latitude than that in the Atlantic.

The longitudinal positions of the Atlantic and Pacific maxima in the lower-tropospheric std dev are very similar except for the temperature where the maxima are some 10° upstream, and the ω_{500} which gives maxima that are also somewhat upstream. The upper-tropospheric maxima occur some 10°–20° downstream of those in the lower troposphere with the Pacific maximum 7°–15° equatorward of the Atlantic maximum, depending on the variable considered. Generally the upper-tropospheric variables show an equatorward shift compared with those in the lower troposphere, of order 6° of latitude in the Atlantic and 10° in the Pacific.

The analyses of Blackmon et al. (1977) and others have shown that there is a suggestion of a third, Siberian storm track near 60°N, 60°–90°E. It is also hinted at by MSLP, V_{850}, and ξ_{850} at T21 resolution, and each of these has a weak local maximum there at T42 resolution. There, T_{850} shows a strong maximum, comparable with the Pacific maximum, whereas ω_{500} has no feature there. The upper-tropospheric fields all show a weak indication of it with the T42 versions of Z, T, and ξ at 250 hPa and θ_{PV2} all having a weak maximum in the region.

The other NH region recognized for its synoptic activity at this time of year is the Mediterranean. In fact Petterssen (1950) gave this region as that with the highest incidence of low pressure centers. The standard MSLP and Z variances, like those shown here, have indicated this merely by a slight bump in the contours at best. However, it is apparent that other variables, which emphasise the smaller synoptic scales that are representative of Mediterranean storms, do pick out the Mediterranean with a std dev maximum. In particular V_{850} and ξ_{850} (and T_{850} at T42 resolution) have a maximum there. The ω_{500} std dev has a significant maximum extending from the eastern Mediterranean through the Middle East. In the upper troposphere, V, ξ, PV_{330}, and θ_{PV2} all show a ridge in their std dev here.

Finally we look further at the T_{850} std dev. The Atlantic maximum is some 50% larger than the Pacific in this field and extends westward into North America. At T42 resolution there is a maximum on the plains on the eastern side of the Rocky Mountains near 53°N. This is only slightly smaller than that near Newfoundland and there is a very sharp minimum in the variance on the western flank of the Rockies. At T42 resolution, V_{850} exhibits a very similar structure in this region. This behavior is consistent with that found by Hsu and Wallace (1985). In fact the Siberian T_{850} std dev maximum commented on previously can also be associated with topography, in this case the Urals to the west and the western and northern flanks of the Himalayas. There is also a weak T_{850} variance maximum to the east of the Himalayas. However, the values over eastern Asia, upstream of the Pacific storm track, are only some 65% of those over North America, upstream of the Atlantic storm track.

4. Feature tracking in the lower troposphere

In this section results from the tracking analysis applied to the various fields is presented and contrasted with the filtered variance perspective.

a. Mean sea level pressure and 850-hPa vorticity

The traditional field for tracking is MSLP, thus results of applying the procedure of Hodges (1995, 1996, 1999) to this field will be presented here. Alongside them will be shown the results for 850-hPa vorticity, a field where the extrema are more prominent and the choice of background field to remove is less important. The 850-hPa vorticity field has also recently been used for tracking studies by Hodges (1996) and by Ayrault and Joly (2000). Comparing these two fields provides a contrast between the two extremes of the feature-scale range. It will be seen below that the results from the two fields are generally similar, though $\boldsymbol{\xi}_{850}$ is better at describing smaller-scale systems and has the advantage of depending on extrapolation below topography in a much smaller area than MSLP.

Eight diagnostics produced from tracking MSLP lows (negative anomalies) are shown in Fig. 5 and from track-

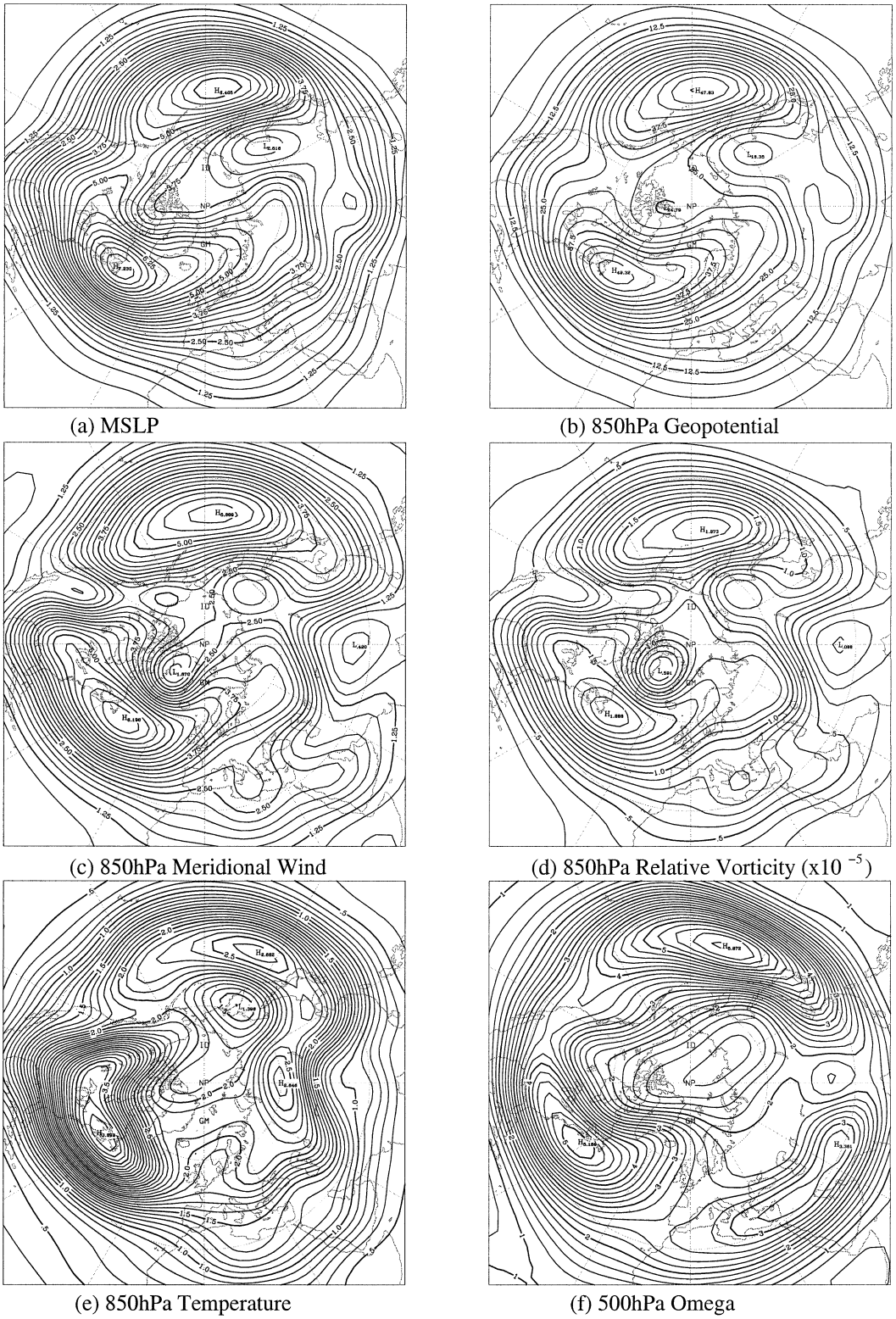

FIG. 3. Lower-tropospheric 2–6-day bandpass filtered variances converted to std dev: (a) MSLP, with contour interval (c.i.) 0.25 hPa, (b) Z_{850}, c.i. 2.5 m, (c) V_{850}, c.i. 0.25 m s^{-1}, (d) ξ_{850}, c.i. 0.1. 10^{-5} s^{-1}, (e) T_{850}, c.i. 0.1 K, (f) ω_{500}, 0.2 hPa h^{-1}. Each filtered field has been smoothed as described in the text.

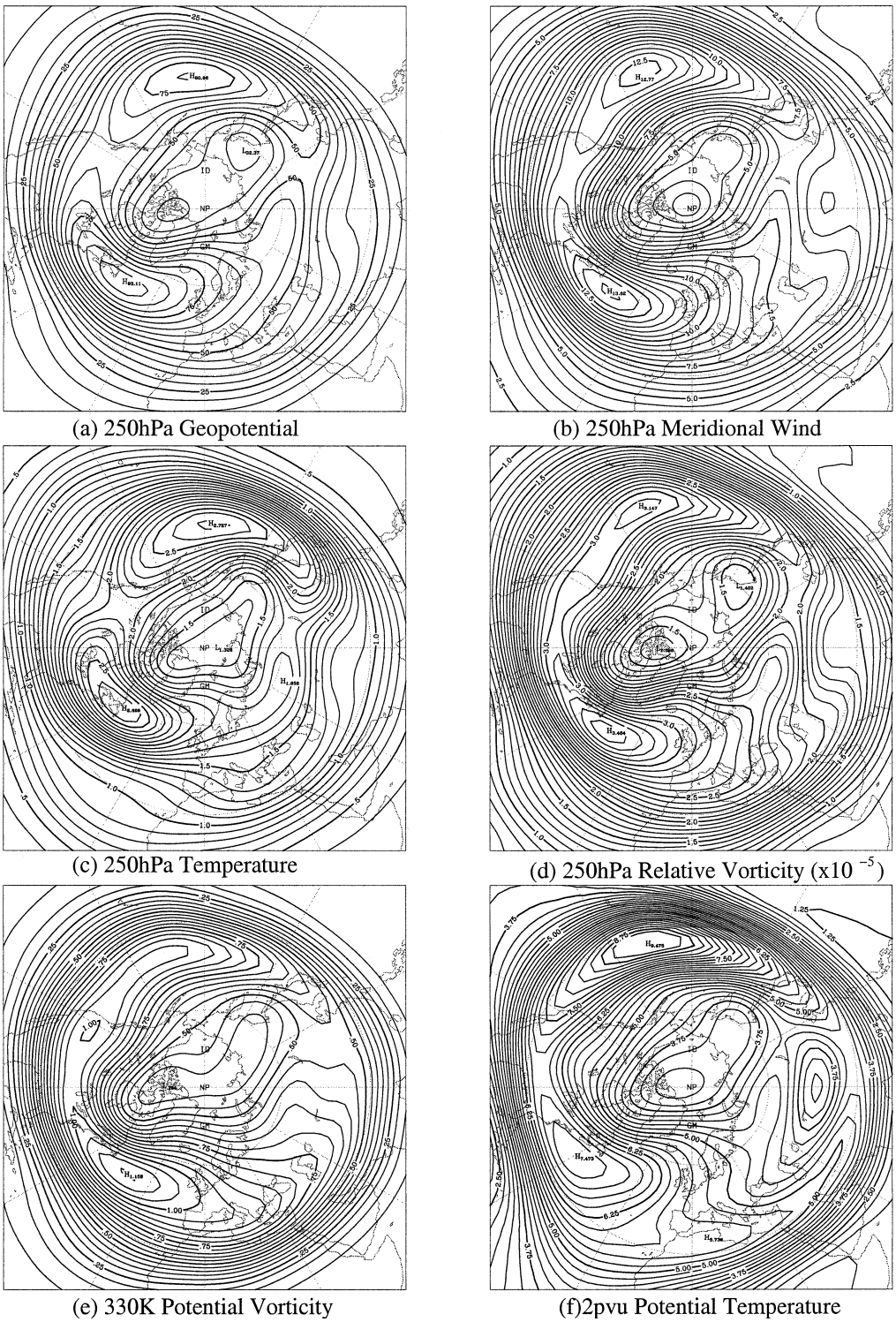

FIG. 4. Upper-tropospheric, smoothed 2–6-day bandpass filtered variances converted to standard deviation: (a) Z_{250}, c.i. 5 m, (b) V_{250}, c.i. 0.5 m s^{-1}, (c) T_{250}, c.i. 0.1 K, (d) ξ_{250}, c.i. 0.1. 10^{-5} s^{-1}, (e) PV$_{330}$, c.i. 0.05 PVU, (f) θ_{PV2}, c.i. 0.25 K.

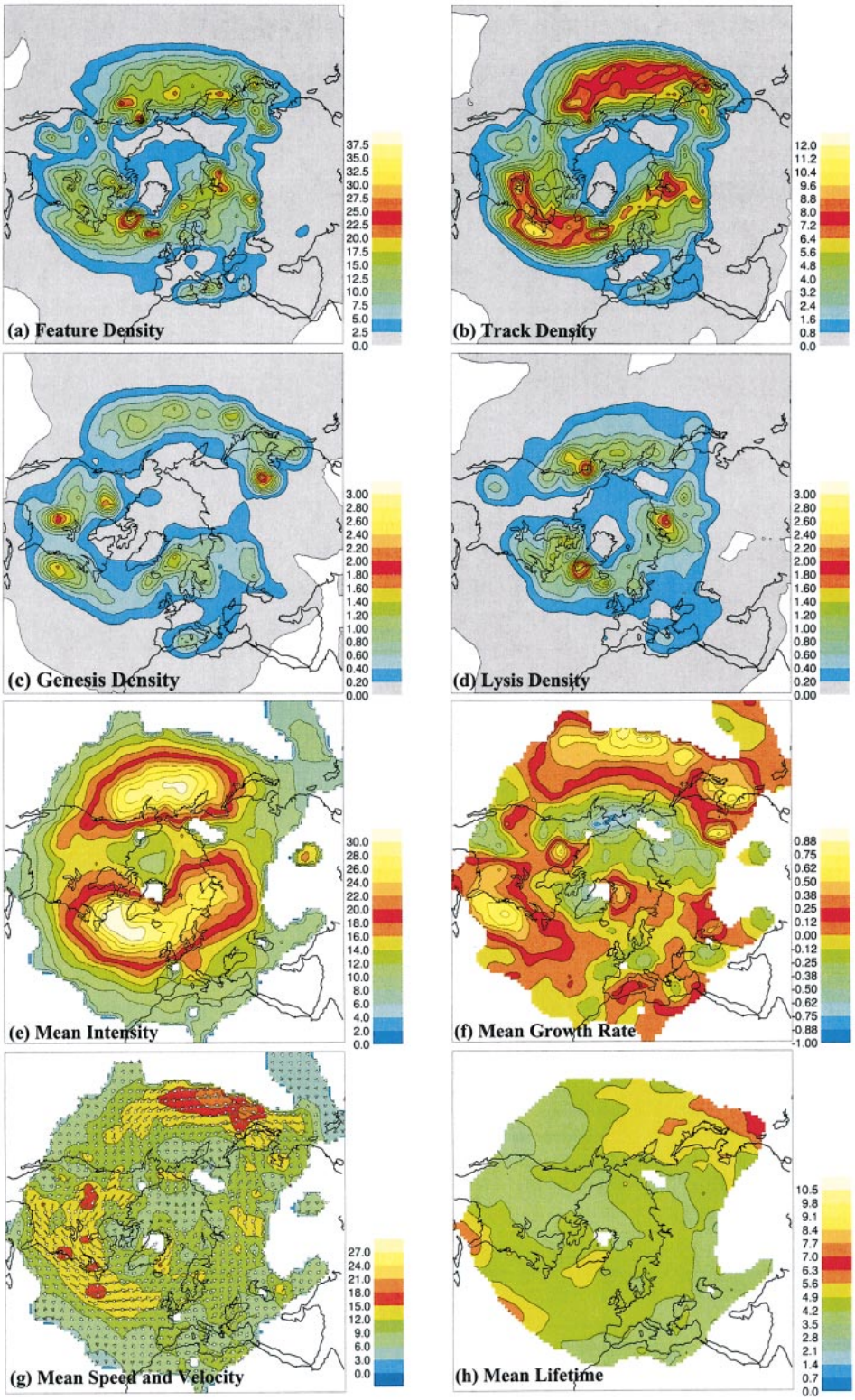

FIG. 5. Attributes for the tracking of negative, cyclonic MSLP features: (a) feature density, (b) track density, (c) genesis density, (d) lysis density, (e) mean intensity (hPa), (f) mean growth rate (day^{-1}), (g) mean velocity (m s^{-1}), and (h) mean lifetime (days). Feature density suppression threshold is 0.5, track density suppression threshold is 0.2.

ing positive vorticity features at 850 hPa in Fig. 6: these focus on the cyclonic activity in these two fields. The first two diagnostics shown are feature density (Figs. 5a, 6a) and track density (Figs. 5b and 6b). The two densities show generally similar features. However, the former is more sensitive to slow moving systems and tends to be dominated by bull's-eyes associated with regions of slow movement. Both fields show track density maxima across the Pacific and from east of the Rockies to Iceland, and also a third, weaker, maximum east of the Urals. The Mediterranean maximum is more marked in vorticity, consistent with Mediterranean storms being relatively small scale, and there is a suggestion of an extension through the Middle East, consistent with the notion suggested by some of the std dev fields described in section 3.

Many aspects of the track density are best looked at in conjunction with the densities of genesis (Figs. 5c, 6c) and lysis (Figs. 5d, 6d), that is cyclogenesis and cyclolysis in this case. Both fields show genesis in Mongolia, and southeast China as previously observed by Chung et al. (1976). Another maximum is found east of Japan and then along the track in the central Pacific. Vorticity shows genesis regions in the lee of the northern and southern Rockies. For MSLP the latter, in particular, is found rather farther downstream. This also occurs in other regions, for example Mongolia, and is a consequence of the systems being identified earlier in their life cycle using vorticity than MSLP. There is genesis also northeast of Cape Hatteras and in the Iceland and Norwegian Sea regions. Other genesis regions are the western Mediterranean and the Caspian Sea. Vorticity also picks up a genesis region to the north of Greenland possibly associated with katabatic winds, which are known to be associated with the generation of vorticity and mesocyclones on the slopes of high orography in polar regions (Heinemann 1998). This is consistent with the fact that this genesis is only seen in the vorticity, pointing to the systems being small scale. The genesis regions off the eastern continental seaboards, near Cape Hatteras and Japan, are the usual baroclinic growth regions as will be apparent by considering the growth rate statistic.

Lysis (Figs. 5d and 6d) occurs on the northern side of the Pacific storm track and then, particularly in vorticity, a strong double maximum on the west coast of North America, near Vancouver Island and the Gulf of Alaska. The Gulf of California lysis maximum, possibly associated with cutoff lows (Bell and Bosart 1989), is placed rather differently in the two fields. There is also a vorticity lysis region from the eastern Great Lakes to the Hudson Bay and extending to Iceland. For MSLP the maximum is on the northeast coast of Canada, on the southern tip of Greenland and south of Iceland. Both fields give lysis in the Norwegian Sea and in Siberia. Both fields also point out separate eastern Mediterranean and Middle Eastern lysis maxima.

To explore further the linkage between genesis, track, and lysis diagnostics, the track and lysis densities have been determined for genesis regions and the genesis and track densities for lysis regions. The analysis is performed by taking the 22-yr track ensemble and extracting all tracks that either start or finish within a 5° spherical cap centered on a genesis or lysis maximum, respectively. The track density and the lysis or genesis densities are computed, respectively, in the same way as for the climatological statistics. Some results of this are shown in Fig. 7 for some of the more interesting examples for genesis and lysis of positive features in ξ_{850}. The positioning of the centers of the spherical caps are given in the legend of Fig. 7. The corresponding MSLP pictures are very similar and not shown. Figure 7a shows the lysis density for positive vorticity features whose genesis is at the western end of the Pacific storm track. The vast majority of those starting over Mongolia finish in eastern China or the Sea of Japan, as observed by Chung et al. (1976). These systems are generally weak (cf. intensity, Fig. 6e) and have been observed to form as secondary systems on the trailing cold fronts of occluded lows in Siberia (Boyle and Chen 1992). Many of the features starting in southeast China finish just to the east of Japan. Even the features starting in the Sea of Japan or to the east of Japan mostly finish in the central or northern Pacific. This raises the question where the features finishing on the west coast of North America originate. The genesis region for these is shown in Fig. 7b, which gives the clear answer that the overwhelming majority of these originate in a secondary development region in the central-eastern Pacific. This region is toward the end of the track of the features originating near eastern Asia. MSLP gives a similar picture of the Pacific storm track being composed of two sections.

The positive vorticity features generated in the lee of the northern and southern Rockies genesis regions have their lysis as shown in Figs. 7c and 7d, respectively. The northern Rockies features have their lysis to the northeast of the Great Lakes and northeast of Canada. The southern Rockies features mostly finish to the south and east of the Great Lakes, with some making it to the south of Greenland. Many of the features starting to the east of Cape Hatteras (Fig. 7e) also finish there but others get through to the Norwegian Sea and western Europe. Finally, the genesis of features whose lysis is in Siberia (Fig. 7f) occurs in a wide area, near the Caspian Sea, east of the Baltic and the Norwegian Seas.

Returning to the negative MSLP and positive 850-hPa vorticity tracking diagnostics, the mean intensities of features are given in Figs. 5e and 6e, respectively. The two variables have perhaps surprisingly similar behaviors. Each shows Pacific and Atlantic storms to have similar mean intensity with weaker storms in northern Asia. The smaller-scale systems occurring in the Mediterranean are seen better in the vorticity as noted before, and they have weaker mean intensities than the main storm track regions. In fact this is a region in which the

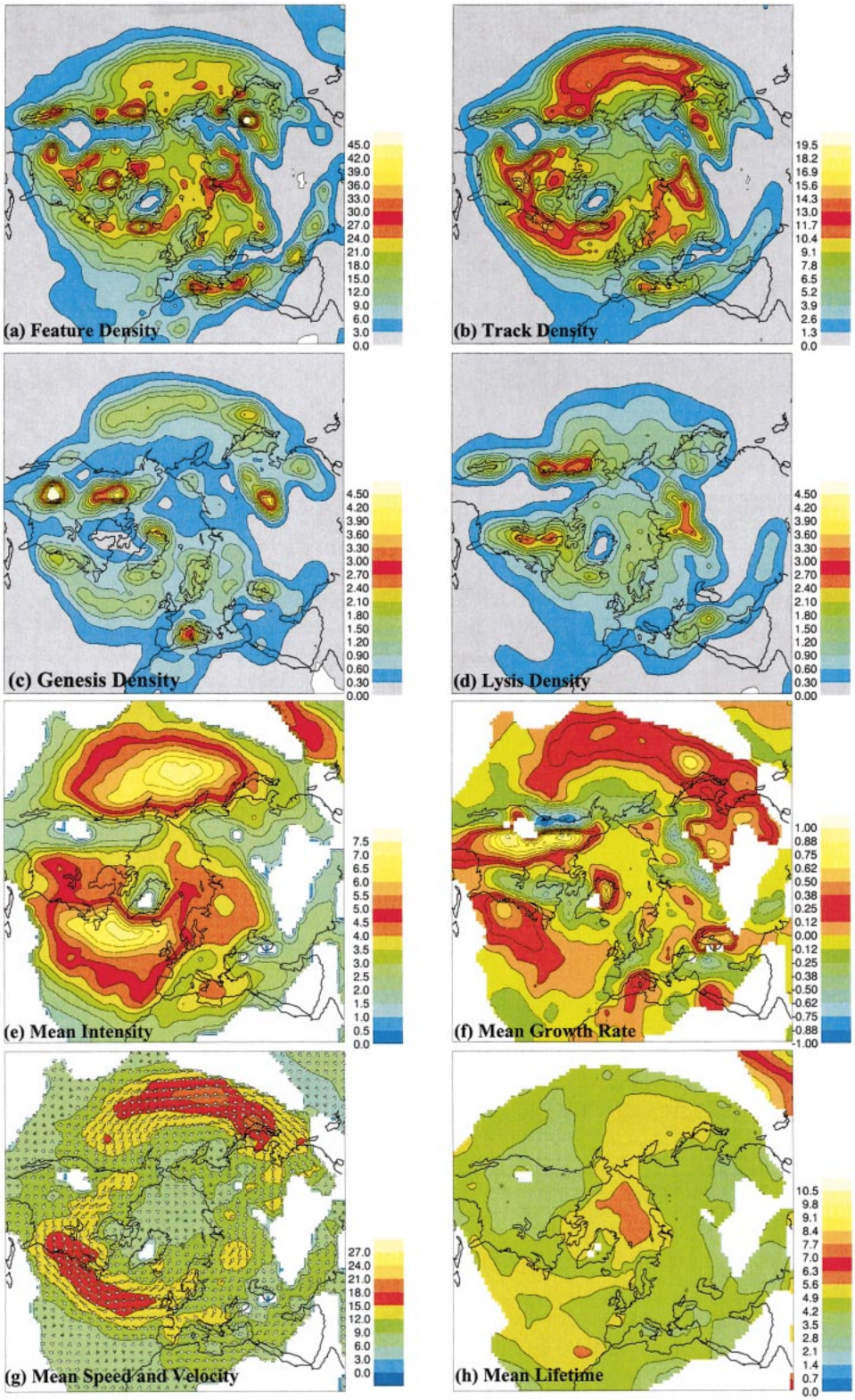

FIG. 6. Attributes for tracking of positive ξ_{850} features. Panels and conventions as in Fig. 5 but with intensity measured in units of $10^{-5}\,s^{-1}$. Feature density suppression threshold is 1.5, track density suppression threshold is 0.5.

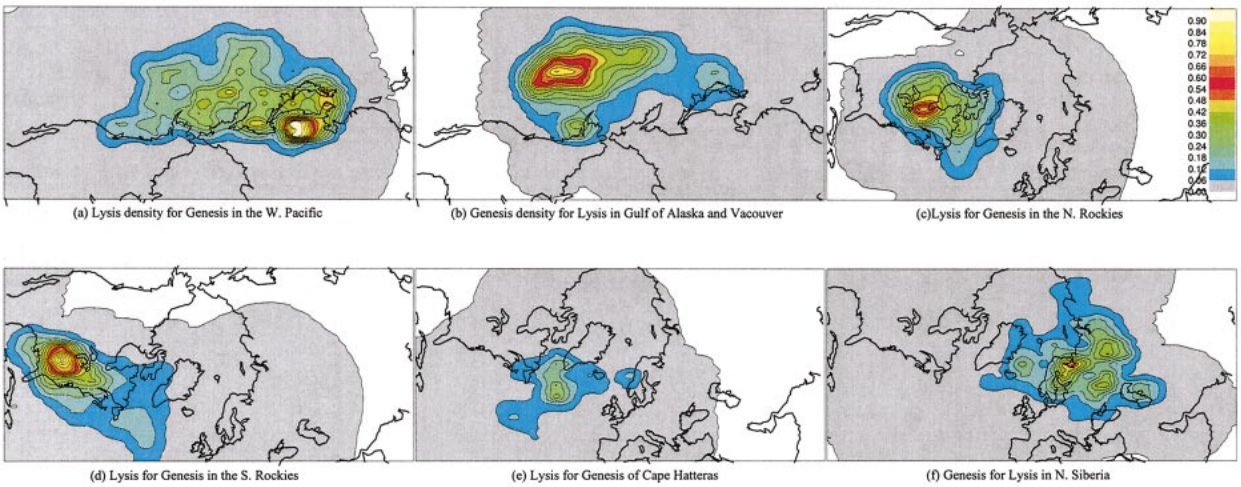

FIG. 7. Lysis and genesis densities for genesis and lysis regions, respectively, for positive ξ_{850} features (refer to Figs. 6c,d): (a) composite map for lysis density for genesis in the western Pacific, just east of Japan, Mongolia, southeast China and Sea of Japan; sampling regions centered at 35°N, 145°E; 47.5°N, 105.5°E; 32.5°N, 115°E; and 37.5°N, 135°E; respectively; (b) composite genesis density for lysis in the Gulf of Alaska and Vancouver Island; sampling regions centered at 57.5°N, 137.5°W and 47.5°N, 125°W respectively; (c) lysis density for genesis in the lee of the northern Rockies; sampling center 60°N, 115°W; (d) lysis density for genesis in the lee of the southern Rockies; sampling center 35°N, 105°W; (e) lysis density for genesis of Cape Hatteras; sampling region 37.5°N, 72.5°W; (f) genesis density for lysis in northern Siberia, sampling regions centered at 60°N, 105°E and 67.5°N, 80°E.

representation of storms are likely to be very sensitive to the integration resolution of the model. The average growth or decay rates of features with amplitude a passing through any location are computed as the mean of $a^{-1}\, da/dt$ and shown in Figs. 5f and 6f. The maximum growth rates are close to $(1\text{-day})^{-1}$ in the main baroclinic regions, but more typically about half this across the rest of the main activity regions of the storm tracks. As discussed in Hoskins (2001), there is surprisingly good agreement between this measure and the Eady maximum growth rate based on linear theory. The Pacific shows growth upstream and along the track with decay to the north and on the west coast of North America associated with the cyclolysis already discussed (cf. Figs. 5d and 6d). For vorticity, the decay on the upslope and growth on the downslope of the Rockies is striking. This is followed for vorticity by decay from the Great Lakes to the Davis Straits, consistent with the lysis there. Both fields show growth off Cape Hatteras and eastward toward the United Kingdom, with lysis to the north and over western Europe.

The mean velocity of features (Figs. 5g and 6g) are generally consistent with steering by the mean flow near the 700-hPa level with maximum speeds occurring from the western continental margins into the two ocean basins consistent with the position and orientation of the two subtropical jets. The mean lifetimes of features (Figs. 5h and 6h) are mostly between 4 and 5 days in the Atlantic consistent with the mean speeds. Lifetimes are rather longer than this in the western Pacific with a decrease in the eastern Pacific consistent with the generation of the secondary systems already discussed.

All these diagnostics have been determined for features of both signs for all the variables whose std dev have been shown in Figs. 3 and 4. However, for the rest of the fields only a small selection will be shown here, concentrating on track densities and mean intensities.

Mobile high pressure systems are less frequently seen and usually less dramatic than low pressure systems identified in the MSLP. Some statistics for them and for negative 850-hPa vorticity features are shown in Fig. 8. Both variables give a Pacific track (Figs. 8a,b) with a density comparable to that for the other sign (Figs. 5e and 6e). However, the intensities (Figs. 8c,d) are considerably smaller. The vorticity (Figs. 8a,c), in particular, shows south-eastward tracks from the northern and central Rockies. There is also a weak track density maximum across the Atlantic, with the largest intensities downstream, centered on the United Kingdom. This is presumably associated with the tendency for blocking-like amplification there. For the MSLP (Figs. 8b,d), the high intensities over the Arctic region, with very few tracks, are related to the poor mean flow removal performed by the planetary waves there (Figs. 2c,d).

b. Other lower-tropospheric fields

At 850 hPa, positive meridional wind can be associated with the warm sectors of storms and negative meridional wind with the cold air behind the systems. This is consistent with there being similar numbers of systems in the track ensembles from both anomaly signs. The track densities and mean intensities for these features are given in Fig. 9. The Pacific storm track is delineated by the tracks for both signs (Figs. 9a,b). The end of the track is characterized by strong positive

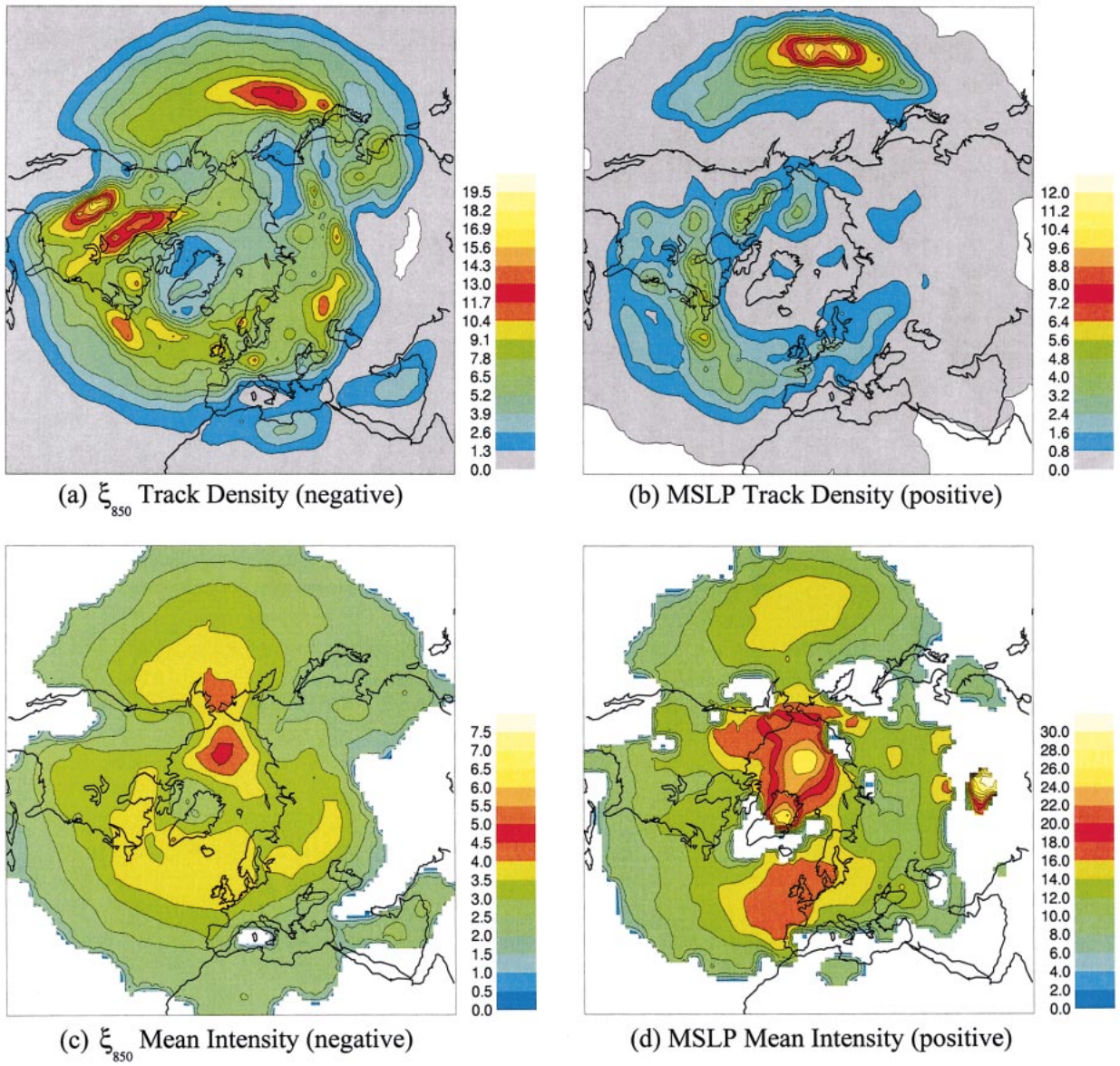

FIG. 8. Attributes for the tracking of negative ξ_{850} features (a) and (c), and positive MSLP features (b) and (d). Shown are track densities (a) and (b) and mean intensities (c) and (d) (units: 10^{-5} s^{-1} and hPa, respectively). Feature density suppression threshold is 1.5 for ξ and 0.5 for MSLP.

(southerly) anomalies. The lee of the Rockies has a very high density for negative (northerly) features with positive features dominating in track and intensity further south. Negative features occur and are strong near northeast Canada. However, positive features dominate along the rest of the Atlantic storm track and into the Norwegian Sea consistent with the frequent occurrence of warm sector flow at the end of this storm track. This feature was also noted above for the Pacific storm track.

Many of these features are reflected in the diagnostics for 850-hPa temperature features given in Fig. 10. The Pacific storm track is evident in features of both signs, with warm features dominant at the west coast of North America. Much more intense features of both signs are found in the lee of the Rockies. Very intense cold features also occur in eastern North America and very intense warm features from Cape Hatteras to the Norwegian Sea. There is also a weak cold track into North Africa and a maximum in cold feature track density from Europe to Siberia. The latter is associated with features generated on the northern side of the track and decaying on the southern side, consistent with this being a region of cold outbreaks. Warm features are found north of the Tibetan Plateau, having moved up its western flank. This was noted above as being a region of high variance in T_{850} (Fig. 3e).

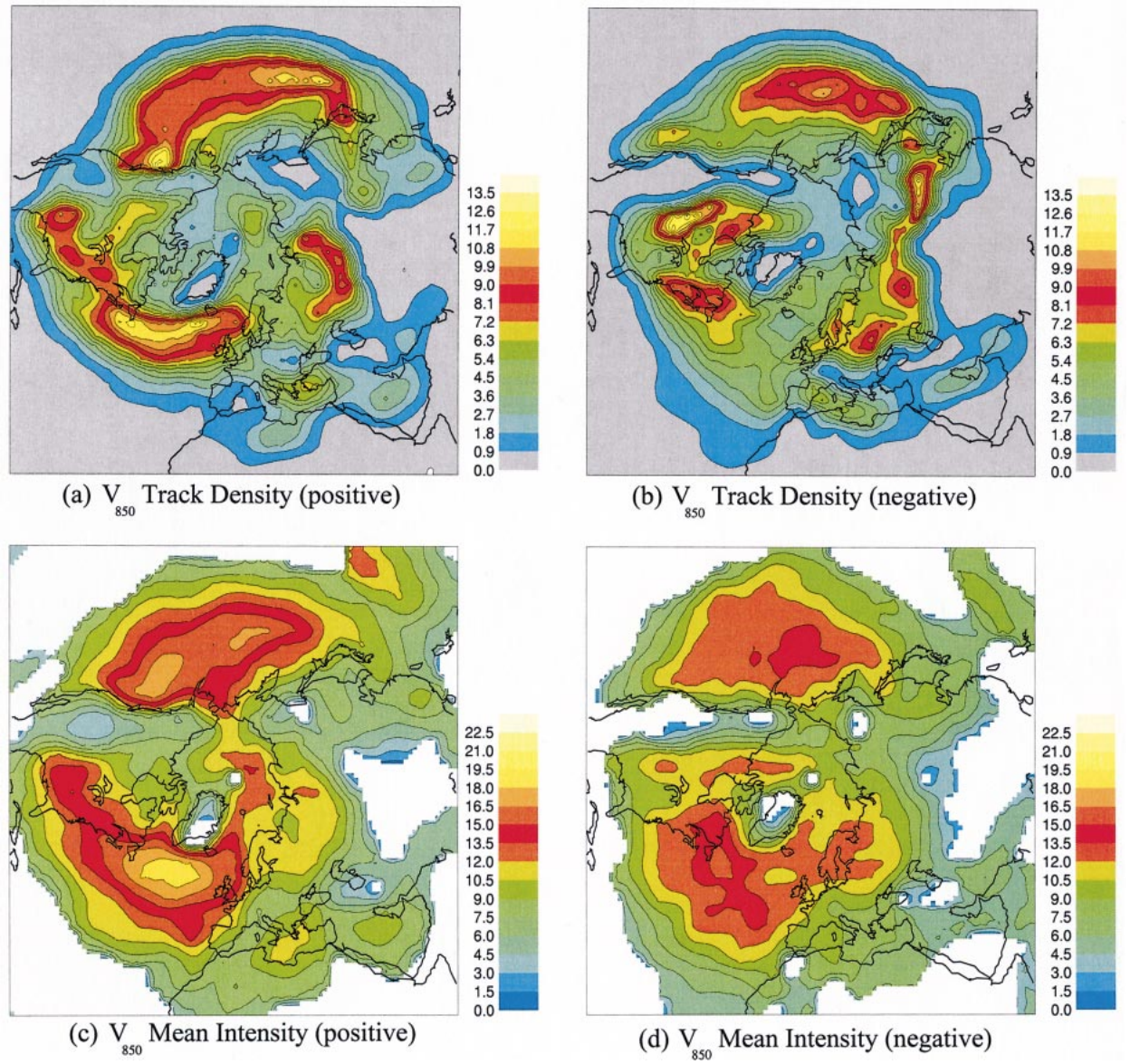

FIG. 9. Attributes for the tracking of positive (a) and (c) and negative (b) and (d) V_{850} features. Shown are track densities (a) and (b) and mean intensities (c) and (d) (units: m s^{-1}). Feature density suppression threshold is 1.0.

The most surprising aspect of the T_{850} diagnostics is the contrasting picture it paints of the two major storm tracks. The Pacific track appears to have small amplitude disturbances on the oceanic baroclinic region. The Atlantic track has very cold air anomalies over North America which decay on the coast or as they flow over the warm waters interacting with the very warm anomalies in air that sweep up from the Sargasso Sea region. The large intensities from the lee of the Rockies to the western Atlantic are consistent with the variance picture (Fig. 3e).

The Z_{850} field will not be discussed in this section as results from tracking systems in this field produce results for the statistics that are very similar to those for MSLP.

Finally as a bridge to section 4c, we consider (Figs. 11a,b) the midtropospheric 500-hPa vertical velocity (ω_{500}). The North Pacific storm track is shown well for features of both signs, with intensities larger than those in the Atlantic. This is consistent with the relative variances in the two regions in this field (Fig. 3f). Descent (positive) features (Fig. 11a) tend to be biased toward subtropical latitudes. There is a marked track for these with large intensities of track density across the southern United States. Significant intensities in track density are also found along the North African jet. Ascent (nega-

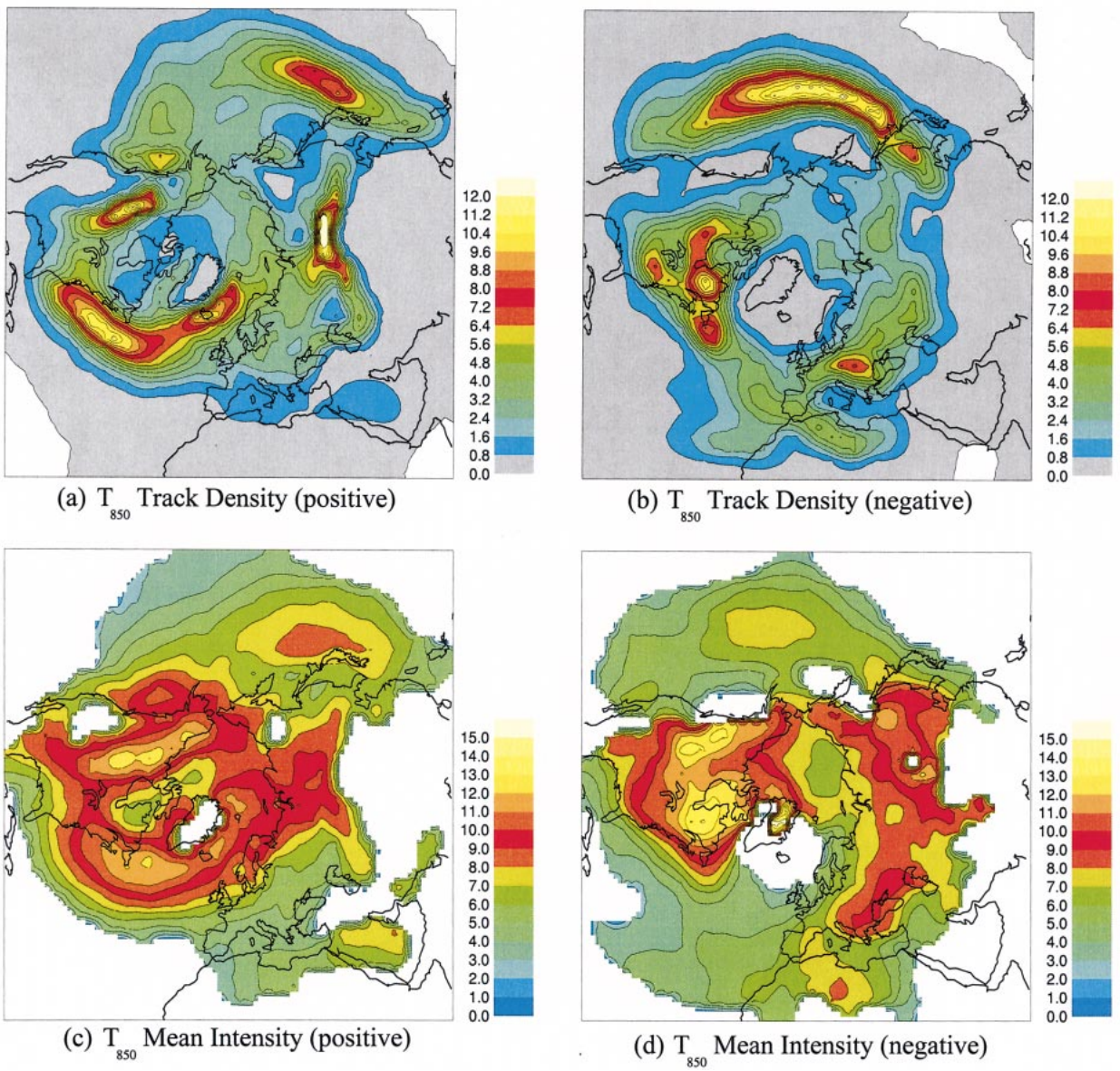

FIG. 10. Attributes for the tracking of positive (a) and (c) and negative (b) and (d) T_{850} features. Shown are track densities (a) and (b) and mean intensities (c) and (d) (units: °C). Feature density suppression threshold is 1.0.

tive) features (Fig. 11b) generally occur in similar regions to those in which lower-tropospheric features are found. The North Pacific storm track now ends on the west coast of North America. Negative features give a North Atlantic track from Cape Hatteras to Iceland. There is high track density but little intensity (not shown) in the Siberian region. There is also a track with significant intensity from the eastern Mediterranean through the Middle East, consistent with the variance maximum there (Fig. 3f).

c. Upper-tropospheric fields

The standard upper-tropospheric variance diagnostic is that for 250-hPa height, and tracking statistics for this are given in Figs. 11c–f. Consistent with the lower-tropospheric concentration on low pressure systems, we first discuss the negative features (troughs, Figs. 11d,f). There is a marked Pacific track with the largest intensities toward the end of it in the central-eastern Pacific. There are intense features over the east coast of North America, but there is little evidence of a North Atlantic storm track. However, there is a marked track from the Mediterranean to the Middle East. The lack of an Atlantic track suggests that the behavior here is very nonlinear with little occurrence of the simple propagation of troughs.

Positive features (ridges, Figs. 11c,e) show only a weak track in the west Pacific, whereas there is a track

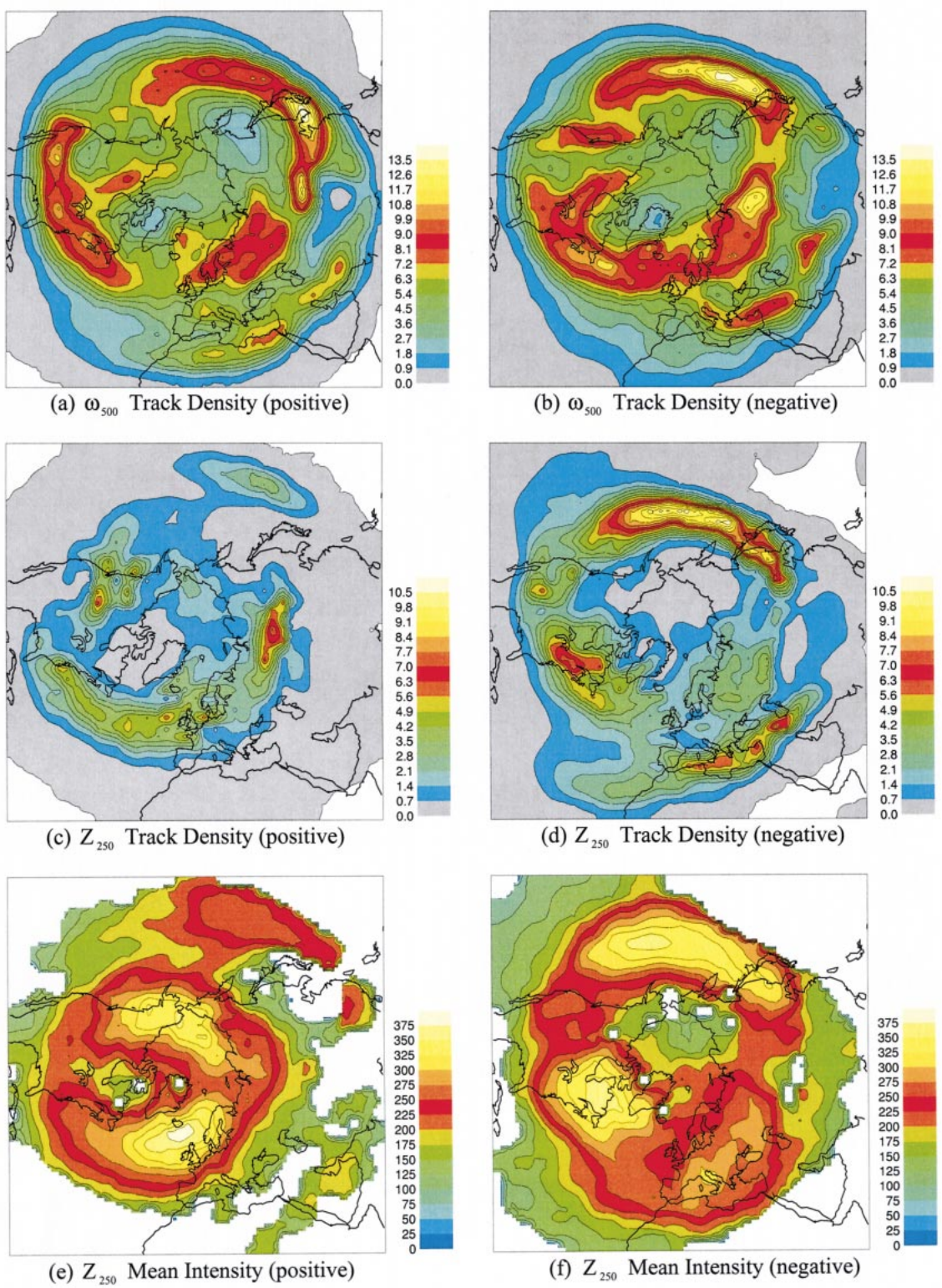

FIG. 11. Track densities for positive (a) and negative (b) ω_{500} features and attributes for the tracking of positive (c) and (e) and negative (d) and (f) Z_{250} features. Track densities for Z_{250} are (c) and (d) and mean intensities are (e) and (f) (units: m). Feature density suppression threshold is 0.5 for Z.

across the North Atlantic with large intensity in the northeast Atlantic. The Siberian track density maximum is accompanied by weaker intensities. It is clear that the similarity of the upper- and lower-tropospheric storm tracks as given by high pass height field variances is much less apparent in tracking diagnostics. Tracking diagnostics applied for 250-hPa meridional wind and temperature (not shown) confirm this.

The results from tracking features in the 250-hPa vorticity (ξ_{250}) and 330-K potential vorticity (PV_{330}) fields yield very similar results to each other. Some diagnostics for the latter are given in Figs. 12a–d. In this case the tracking of positive features, corresponding in general to pressure troughs, shows large intensities (Fig. 12c) near the subtropical jet from the mid-Pacific eastward through the Mediterranean. The track density (Fig. 12a) picks out the region across North America and from the east Atlantic through the Middle East. In Anderson et al. (2001b, manuscript submitted to *J. Climate*, hereafter AHHb) it will be shown that there is evidence that the lack of tracks recorded in the west Pacific is to a certain extent associated with their rejection on the track smoothness criterion. The features occurring there in the ERA-15 analysis do not show good temporal continuity in their positions with multiple feature points for the same system occurring often. Both the NCEP reanalysis (restricted to the 1979–99 period) and post-ERA-15 ECMWF operational analyses (1994–2000/2001) show much better coherence here, with consequently more tracks in the west and central Pacific and also more generally. The results shown in Figs. 12a–d combine those from both the ERA-15 and operational analyses and thus reflect the contribution from the longer ERA-15 time period. For example, the track densities for positive features in PV_{330} and ξ_{250} from the NCEP reanalysis are given in Figs. 12e and 12f, respectively. Comparison of the former with the Fig. 12a results shows the much larger number of systems that are tracked, in particular in the west Pacific. This is also the case for the ξ_{250}. This lack of coherence for PV_{330} and ξ_{250} as ERA is most prevalent during both NH and SH winters when upper troposphere winds and shear are at their strongest.

This apparent sensitivity to the analysis system could possibly be associated with the use of the more sophisticated data assimilation schemes used by NCEP (3D Var) and for the ECMWF operational analyses (from 1994 3D Var was used and since 1999, 4D Var has been in operational use) as opposed to the OI used in ERA-15. Further evidence for this comes from the GEOS-1 reanalysis data (1980–93). At the 250-hPa level the vorticity (not displayed here) shows results comparable with both NCEP and the ECMWF operational analyses. The GEOS-1 system is based on a finite difference model (both NCEP and ECMWF are based on spectral models) and uses a form of OI data assimilation (Schubert et al. 1995). The difference between the form of OI used in ERA-15 and GEOS-1 is the way the observations are used, particularly with respect to the upper-air observations. The GEOS-1 system uses an incremental analysis update approach where an OI analysis is performed at the analysis time to compute analysis increments that are then gradually incorporated into a rerun forecast. This has the effect of smoothing out the incorporation of the observations. ERA-15 used a form of intermittent OI. Of course, there are many other differences between the systems used to produce the various reanalyses in terms of spatial resolution, model physics, and observations used which might have an impact on the synoptic systems. This should be explored further. However, it appears in general that the variational schemes (3D Var, 4D Var) are better able to use the sparse observations from sondes and profilers at this level resulting in more coherent structures, particularly in the small-scale fields.

Negative ξ_{250} and PV_{330} features (Figs. 12b,d) generally show little sign of coherent tracks with significant intensity. The largest intensities are found at the end of the two storm tracks.

The overall picture given by PV tracking is rather different from that suggested by its high pass std dev (Fig. 4e). Even so there is still an indication that PV features from the Pacific could feed the North Atlantic storm track. There is also a suggestion that features in the North African–Asian subtropical jet could feed the North Pacific storm track. This picture is clearer in the NCEP reanalysis track densities for positive, cyclonic features in the PV_{330} and ξ_{250} fields (Figs. 12e,f).

Tracking applied to potential temperature on the PV $= 2$ PVU surface supports this suggestive picture. The positive features (Figs. 13a,c), generally corresponding to anticyclonic structures, show large intensity in the subtropics but weak track organization there, and conversely north of Tibet. It should be recalled that the nature of this field favors subtropical latitudes somewhat. It is the negative, cyclonic, features (Figs. 13b,d) that are reflected in the variance field (Fig. 4f). The overall impression is of a single spiraling track from the southeastern North Atlantic, eastward across Asia, the Pacific, and North America, and into the northeastern North Atlantic. There is an organized track with large mean intensity in northern North Africa and extending through the Middle East. There is also a suggestion of feeding the Pacific storm tracks from here and from a northern branch. The Pacific storm track is well organized with large intensity. It weakens toward the east Pacific but there is a reinvigoration on the west coast of North America, feeding through to the North Atlantic storm track. The track density is suggestive of some organization also across northern Eurasia where positive features were well organized and extend down into Mongolia.

5. Discussion

The determination of synoptic timescale std dev pictures for a wide range of variables has given a rich

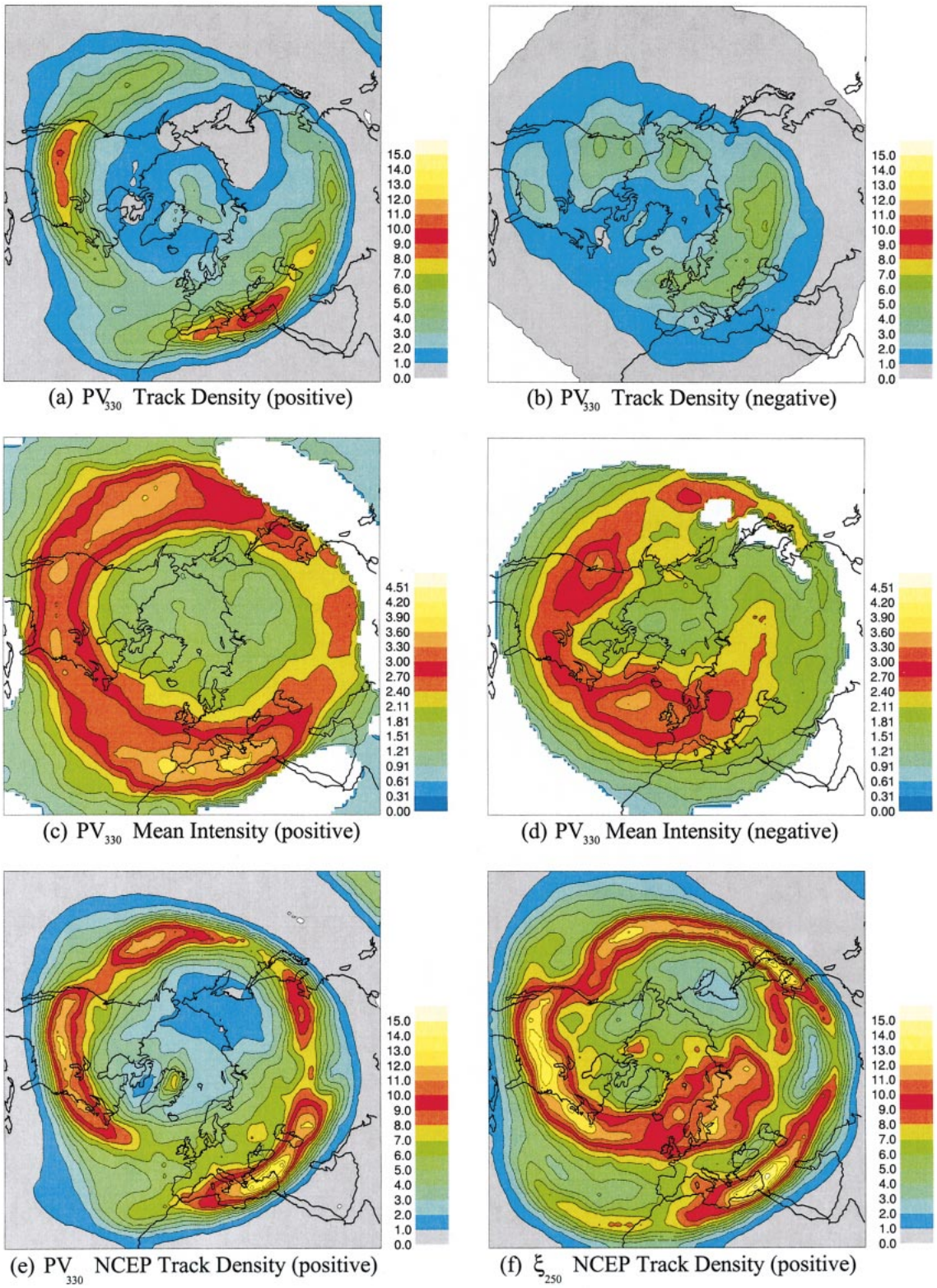

FIG. 12. Attributes for the tracking of positive (a) and (c) and negative (b) and (d) PV_{330} features. Shown are track densities (a) and (b) and mean intensities (c) and (d). Also track densities for positive, cyclonic features in (e) PV_{330} and (f) ξ_{250} using NCEP reanalysis data. Feature density suppression threshold is 0.5 for PV.

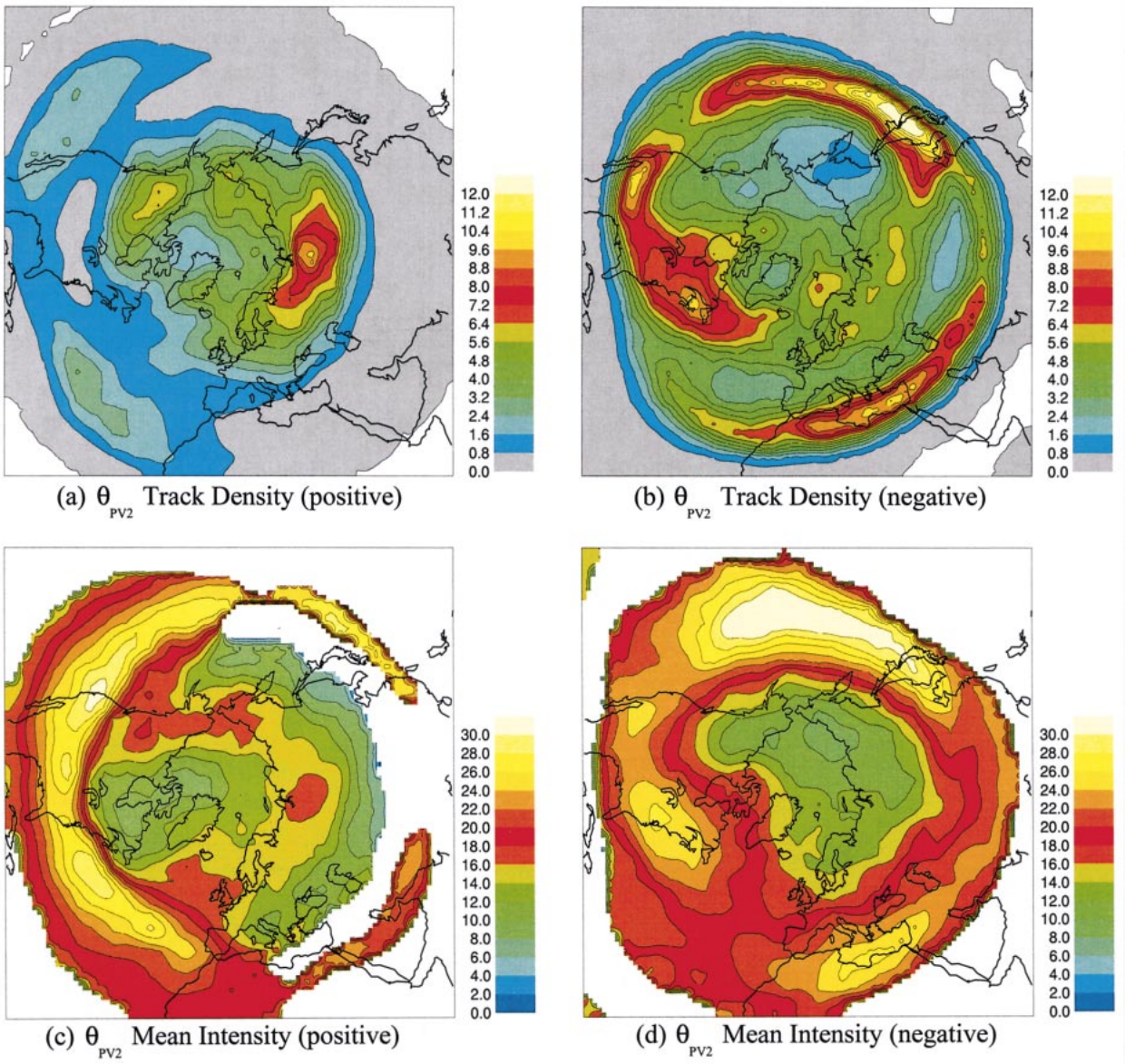

FIG. 13. Attributes for the tracking of positive (a) and (c) and negative (b) and (d) θ_{PV2} features. Shown are track densities (a) and (b) and mean intensities (c) and (d) (units: K). Feature density suppression threshold is 0.5.

picture of the nature and comparative magnitudes of the North Pacific and North Atlantic storm tracks, and of the Siberian and Mediterranean candidates for storm tracks. For example, although most variables give the Atlantic storm track to be stronger than the Pacific, 850-hPa Z, V, and ξ make them about equal, and θ_{PV2} gives the Pacific storm track as stronger. The middle- and upper-tropospheric fields show a region of enhanced variance from the Mediterranean through the Middle East. However, most of the features of note in the variances are more vividly seen in the tracking of positive and negative features in these fields. This is the case, despite the fact that anticyclonic features that are mobile and have a smooth track are not found as frequently as cyclonic features with these qualities.

Considering briefly the anticyclonic features, the mid-Pacific was evident in lower-tropospheric variables and the west coast of North America in upper-tropospheric variables. All of them picked out the east Atlantic–northwest European region. Upper-tropospheric features also highlighted the Siberian region north of Tibet.

A subjectively determined summary of the tracks of cyclonic features in the upper and lower troposphere is given in Fig. 14. This is based in particular on the results for negative θ_{PV2} (Figs. 13b,d) and positive ξ_{850} (Fig.

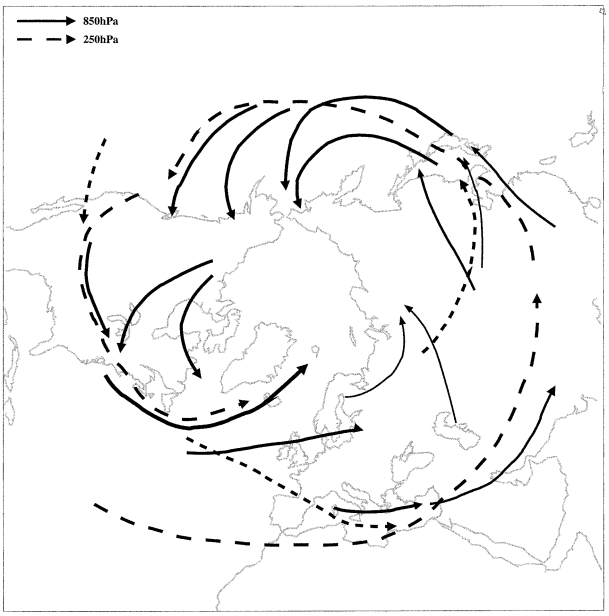

FIG. 14. Schematic of principal tracks for lower- (solid line) and upper- (dashed line) tropospheric storm track activity based on ξ_{850} and θ_{PV2}.

6). Interesting speculations can be made on the basis of this. The band starting in the subtropical eastern North Atlantic and spiraling around the hemisphere in the upper troposphere could provide a source of perturbations that amplify through the depth when the lower-tropospheric conditions are favorable. This occurs sequentially in the western Mediterranean, southeast China, to the east of Japan, in the central-east Pacific, east of the southern Rockies, and off Cape Hatteras, the usual baroclinic regions. The downstream coupling in the Siberian region also appears to feed upper-level perturbations that amplify in the Mongolian region. A similar picture in the upper troposphere is indicated by the results of Chang and Yu (1999) when they sought the regions in which there is evidence of the downstream propagation of activity in wave packets.

It has been found that very few synoptic systems can be tracked along the length of the Pacific storm track. Indeed, most of the systems generated over eastern Asia do not even reach the mid-Pacific. It is the systems that are generated in the central-east Pacific that occlude on the northwest coast of North America.

As well as the southern Rockies lower-tropospheric generation region, there is also a northern Rockies region. The only evidence of feeding in the upper troposphere here is by anticyclonic features tracked from the west. Most of the systems generated in both regions do not get very far into the Atlantic and it was the systems generated off the east coast that generally moved into the northwestern Atlantic.

The third, Siberian storm track, with the Ural Mountains to the west and the Tibetan plateau to the southeast, appears to be strongly influenced by these topographic features. It is the meeting place of storms generated in the Norwegian Sea and Baltic Sea to the northwest and the Caspian Sea to the southwest.

Systems generated in the western Mediterranean generally finished in the eastern Mediterranean but the storm track does continue through Syria by means of storms mostly generated in the eastern Mediterranean.

Lower-tropospheric temperature anomaly tracking has suggested a marked contrast between the Pacific and Atlantic storm tracks. The picture given here is that the North Pacific storm track has a temperature field dominated by ripples on the baroclinic region across the ocean, whereas the North Atlantic storm track entrance region is a confluence of strong thermal anomalies originating in widely different regions. Very strong cold anomalies originate over the Canadian Arctic and decay as they are influenced by the warm waters of the Atlantic. The warm anomalies originate over the Sargasso Sea and move along the storm track.

Generally speaking, the features discussed in this paper are thought to be fairly robust with respect to the background flow that is removed. As will be shown in AHHa, as even more is removed, the statistics for positive and negative features become more similar. In particular the asymmetry between the warm and cold air behavior at the entrance of the North Atlantic storm track becomes less. However, the essence of the differing thermal pictures of the two storm tracks is likely to remain.

The diagnostics described here have also been performed on the extended ERA-15 data for both hemispheres and for all four seasons, and for North Atlantic Oscillation and Pacific–North America teleconnection stratified data. In future publications, aspects of these results will be described as well as a fuller comparison between various reanalyses datasets [ERA-15, NCEP I, NCEP Department of Energy (NCEP II DOE), and GEOS-1]. A comparison of the behavior of a high-resolution GCM (the Met Office Unified Model) with that of the ERA-15 data will be given in AHHb.

Acknowledgments. We acknowledge the efforts of Rex Gibson and the ERA team at ECMWF in creating the reanalysis data used in this study and Paul Berrisford in making it available to us. For the NCEP data, thanks go to the Climate Diagnostics Center (CDC) for making the pressure level data available and to NCAR for supplying the NCEP PV data. The GEOS1 data were supplied by the Goddard Space Flight Center Distributed Active Archive Center. This research was in part supported by the EC Environment and Climate Research Programme Contract ENV4-CT97-0499, Climate and Natural Hazards.

REFERENCES

Ayrault, F., and A. Joly, 2000: L'Origine des Dépressions Météorologiques sur l'Atlantique: Nouvelle Perspective Climatologique.

Compt. Rend. Acad. Sci. Paris, Earth Planet. Sci., **330,** 173–178.

Bell, G. D., and L. F. Bosart, 1989: A 15-year climatology of Northern Hemisphere 500 mb closed cyclone and anticyclone centers. *Mon. Wea. Rev.*, **117,** 2142–2163.

Berbery, E. H., and C. S. Vera, 1996: Characteristics of the Southern Hemisphere winter storm track with filtered and unfiltered data. *J. Atmos. Sci.,* **53,** 468–481.

Blackmon, M. L., 1976: A climatological spectral study of the 500 mb geopotential height of the Northern Hemisphere. *J. Atmos. Sci.,* **33,** 1607–1623.

——, J. M. Wallace, N.-C. Lau, and S. L. Mullen, 1977: An observational study of the Northern Hemisphere wintertime circulation. *J. Atmos. Sci.,* **34,** 1040–1053.

Blender, R., K. Fraedrich, and F. Lunkeit, 1997: Identification of cyclone track regimes in the North Atlantic. *Quart. J. Roy. Meteor. Soc.,* **123,** 727–741.

Boyle, J. S., and T. J. Chen, 1992: Synoptic aspects of the winter East Asia monsoon. *Monsoon Meteorology, Oxford Monogr. Geol. Geophys.*, No. 7, Oxford University Press, 125–160.

Chang, E. K. M., and D. B. Yu, 1999: Characteristics of wave packets in the upper troposphere. Part I: Northern Hemisphere winter. *J. Atmos. Sci.,* **56,** 1708–1728.

Chung, Y.-S., K. D. Hage, and E. R. Reinelt, 1976: On lee cyclogenesis and airflow in the Canadian Rocky Mountains and the East Asian mountains. *Mon. Wea. Rev.,* **104,** 879–891.

Gibson, J. K., P. Kållberg, S. Uppala, A. Hernandez, A. Nomura, and E. Serrano, 1997: ERA description. ECMWF Re-Analysis Project Report Series, No. 1, ECMWF, Reading, United Kingdom, 71 pp.

Hayden, B. P., 1981: Cyclone occurence mapping: Equal area or raw frequencies? *Mon. Wea. Rev.,* **109,** 168–172.

Heinemann, G., 1998: Katabatic wind and boundary layer front experiment around Greenland (''KABEG '97''). Rep. on Polar Research 269, Alfred-Wegener-Institut für Polar und Meeresforschung, 93 pp.

Hodges, K. I., 1994: A general method for tracking analysis and its application to meteorological data. *Mon. Wea. Rev.,* **122,** 2573–2586.

——, 1995: Feature tracking on the unit sphere. *Mon. Wea. Rev.,* **123,** 3458–3465.

——, 1996: Spherical nonparametric estimators applied to the UGAMP model integration for AMIP. *Mon. Wea. Rev.,* **124,** 2914–2932.

——, 1999: Adaptive constraints for feature tracking. *Mon. Wea. Rev.*, **127,** 1362–1373.

Hoskins, B. J., 1997: A potential vorticity view of synoptic development. *Meteor. Appl.,* **4,** 325–334.

——, 2001: Cyclones and storm-tracks. *Quart. J. Roy. Meteor. Soc.*, **127,** in press.

——, and P. D. Sardeshmukh, 1984: Spectral smoothing on the sphere. *Mon. Wea. Rev.,* **112,** 2524–2529.

——, and P. Berrisford, 1988: A potential vorticity perspective on the storm of 15–16 October 1987. *Weather,* **43,** 122–129.

——, H. H. Hsu, I. N. James, M. Masutani, P. D. Sardeshmukh, and G. H. White, 1989: Diagnostics of the global atmospheric circulation based on ECMWF analyses 1979–1989. UGAMP Tech. Rep. 7, Dept. of Meteorology, University of Reading, 217 pp.

Hsu, H.-H., and J. M. Wallace, 1985: Vertical structure of wintertime teleconnection patterns. *J. Atmos. Sci.,* **42,** 1693–1710.

Kalnay, E., and Coauthors, 1996: The NCEP/NCAR 40-Year Reanalysis Project. *Bull. Amer. Meteor. Soc.*, **77,** 437–471.

Kay, S. M., 1988: *Modern Spectral Estimation—Theory and Application.* Prentice-Hall, 543 pp.

Klein, W. H., 1957: Principal tracks and mean frequencies of cyclones and anticyclones in the Northern Hemisphere. Research Paper 40, U.S. Weather Bureau, 60 pp.

Lefevre, R. J., and J. W. Nielsen-Gammon, 1995: An objective climatology of mobile troughs in the Northern Hemisphere. *Tellus,* **47A,** 638–655.

Murray, R. J., and I. Simmonds, 1991a: A numerical scheme for tracking cyclone centers from digital data. Part I: Development and operation of the scheme. *Aust. Meteor. Mag.,* **39,** 155–166.

——, and ——, 1991b: A numerical scheme for tracking cyclone centers from digital data. Part II: Application to January and July GCM simulations. *Aust. Meteor. Mag.,* **39,** 167–180.

Nakamura, H., 1992: Midwinter suppression of baroclinic wave activity in the Pacific. *J. Atmos. Sci.,* **49,** 1629–1642.

Petterssen, S., 1950: Some aspects of the general circulation. *Centennial Proc. Royal Meteorological Society,* Oxford, United Kingdom, Roy. Meteor. Soc., 120–155.

Schubert, S., and Coauthors, 1995: A multiyear assimilation with the GEOS-1 system: Overview and results. NASA Tech. Memo. 104606, Vol. 6, 183 pp.

Serreze, M. C., F. Carse, R. G. Barry, and J. C. Rogers, 1997: Icelandic low cyclone activity: Climatological features, linkages with the NAO, and relationship with recent changes in the Northern Hemisphere circulation. *J. Climate,* **10,** 453–464.

Simmonds, I., and K. Keay, 2000: Mean Southern Hemisphere extratropical cyclone behavior in the 40-Year NCEP–NCAR Reanalysis. *J. Climate,* **13,** 873–885.

Sinclair, M. R., 1994: An objective cyclone climatology for the Southern Hemisphere. *Mon. Wea. Rev.,* **122,** 2239–2256.

Taylor, K. E., 1986: An analysis of biases in traditional cyclone frequency maps. *Mon. Wea. Rev.,* **114,** 1481–1490.

Wallace, J. M., G. H. Lim, and M. L. Blackmon, 1988: Relationship between cyclone tracks, anti-cyclonic tracks, and baroclinic waveguides. *J. Atmos. Sci.,* **45,** 439–462.